Journal of Applied Physics ARTICLE scitation.org/journal/jap

Back-surface recombination, electron reflectors, and paths to 28% efficiency for thin-film photovoltaics: A CdTe case study

Cite as: J. Appl. Phys. **125**, 053101 (2019); doi: 10.1063/1.5063799
Submitted: 1 October 2018 · Accepted: 13 January 2019 ·
Published Online: 1 February 2019

Joel N. Duenow and Wyatt K. Metzger

AFFILIATIONS

National Renewable Energy Laboratory, 15013 Denver West Pkwy., Golden, Colorado 80401, USA

ABSTRACT

As thin-film and silicon solar technologies mature, questions emerge about the upper bounds of thin-film solar performance and realistic experimental paths to reach them. Directions include increasing absorber hole density and bulk lifetime, improving the junction interface, reducing back-surface recombination, and implementing a back-surface electron reflector. Textbook solutions of idealized p-n junctions create a powerful conceptualization of solar cells as predominantly minority-carrier-driven devices. We demonstrate that thin films are distinct, and models often fail to capture the important role of majority-carrier lifetime, leading to contradictions with lifetime measurements and overestimates of potential device improvement from back-surface passivation and/or reflectors. Furthermore, we identify methods to probe majority-carrier lifetime and re-examine the degree to which back-surface passivation and electron reflectors can increase efficiency for a range of common thin-film interface and absorber properties, using current and emerging CdTe technology as an example. Results indicate that a practical approach is to focus first on improving front-interface recombination velocity and the absorber properties, and then on implementing the back-surface passivation or reflector, which can ultimately allow thin-film solar technology to reach 28% efficiency.

I. INTRODUCTION

CdTe, Cu(In,Ga)Se_2 (CIGS), perovskites, and multicrystalline Si have all reached similar record photovoltaic (PV) cell efficiencies of 22%–23%.[1] $Cu_2ZnSn(S,Se)_4$, high-growth-rate III-Vs, and new absorbers may approach these values in the future.[2,3] These technologies offer distinct processing and cost-structure potential to the predominant Si technologies. Thin-film CdTe solar technology is producing electricity at costs competitive with conventional fuels today.[4,5] For thin-film technologies to reach their full potential, paths to achieve cell efficiency beyond 25% are critical.

Collecting significant photocurrent is suited to strongly absorptive thin films. In the case of CdTe-based PV, photocurrent has been nearly maximized by transitioning away from absorptive buffers (CdS), optimizing front-stack optics, and implementing a graded $CdSe_xTe_{1-x}$ alloy within the absorber.[6–8] Hole density has historically been limited by intrinsic defect chemistry and compensation to 10^{13}–10^{15} cm^{-3}, in part by implementing $CdCl_2$ and Cu. Aggregate carrier lifetime from interface, grain-boundary, and grain-interior recombination has been limited to several ns. For these material characteristics, the upper fill factor (FF) limit of about 80% has already been achieved.[6,9,10] Consequently, a remaining path to improve performance is to increase the open-circuit voltage (V_{oc}) by increasing the hole density and lifetime by orders of magnitude.[10–12] This then allows further increasing FF beyond 85% and efficiency toward 25%.[10]

Experimental efforts are establishing the groundwork for this path. It was recently shown that single-crystal (SX) CdTe can achieve hole densities greater than 10^{16} cm^{-3} simultaneously with radiatively limited lifetimes of hundreds of ns, commensurate with values for GaAs.[13] When SX p-type absorbers were placed into otherwise traditional polycrystalline (PX) film stacks, CdTe V_{oc} exceeded the historic 1-V barrier.[13] SX research will continue to be important to establish novel interfaces, absorber properties, back contacts, device integration, and proof of concept in the future.[14] At the same time, work is ongoing to integrate both lifetime and hole-density improvements into PX CdTe-based cells.

For example, recent articles have demonstrated hole densities exceeding 10^{16} cm^{-3} in PX films,[15–17] and expanding grain size and shifting to $CdSe_xTe_{1-x}$ has increased bulk lifetimes to tens of ns in devices and hundreds of ns in PX double heterostructures.[18–21] Both perovskites and CIGS have also shown long lifetimes, with hole densities ranging from intrinsic to about 10^{16} cm^{-3}.[22,23] Recent simulation results demonstrate that once improved hole density and lifetime are in place, front-interface and grain-boundary passivation can enable 25% efficiency.[10]

However, controlling front-interface and absorber properties is experimentally difficult. Therefore, it is important to understand when back-surface passivation and reflectors can significantly improve performance, and when they should be pursued in lieu of or in parallel with absorber and front-interface work. For example, in CdTe PV, the back-contact region has very poor lifetime—on the order of tens to hundreds of ps—so back-surface passivation may be useful. Alternatively or in parallel to passivation, implementation of a back-surface reflector (BSR) using a layer of expanded bandgap (e.g., $Cd_{1-x}Zn_xTe$ or $Cd_{1-x}Mg_xTe$) to reflect electrons has been suggested as an approach to improve V_{oc} beyond 1 V in PX films.[11,24] Because CdTe, $CdSe_xTe_{1-x}$, and other thin films continue to demonstrate hole density and lifetime improvements, it has become increasingly important to understand when back-surface improvement may lead to substantively enhanced current-voltage characteristics. In this work, we quantify the degree to which back-surface reflection and passivation improve performance as a function of absorber and interface properties to guide development toward 28% efficiency.

II. PHYSICAL MODEL

The CdTe PV device structure is similar to that of many planar thin-film technologies. The model [Fig. 1(a)] consists of an idealized transparent front electrode, intrinsic SnO_2, a 10-nm-thick CdS buffer, a 3-μm-thick CdTe absorber, an optional 100-nm-thick BSR layer, and an ohmic back contact. Material input values are described in Ref. 10 and a table in the supplementary material. The CdTe hole densities are varied from 10^{13} cm^{-3} to 10^{16} cm^{-3}. 10^{13} cm^{-3} is at the low end of measured values and considered an option for p-i-n structures. 10^{14} cm^{-3} is more typical of the current state-of-the-art using $CdCl_2$ treatments and Cu. 10^{16} cm^{-3} represents recently improved hole density in PX films doped with group V (GrV) dopants.[25,26] The effects of varying electron (minority) and hole (majority) carrier lifetime values are investigated together with different front (S_{front}) and back (S_b) interface recombination velocities. Absorber thickness is not evaluated here. The barrier height (φ_e) of the BSR, varied between 0 and 0.2 eV, is accommodated in the conduction band [Fig. 1(b)].[24] The results presented correspond to an ohmic back contact and do not change for back-contact barrier heights up to 0.3 eV (not shown). Marginal V_{oc} shifts commence for barriers approaching 0.4 eV and become significant at 0.5 eV. These effects are caused primarily by hole impedance at the back

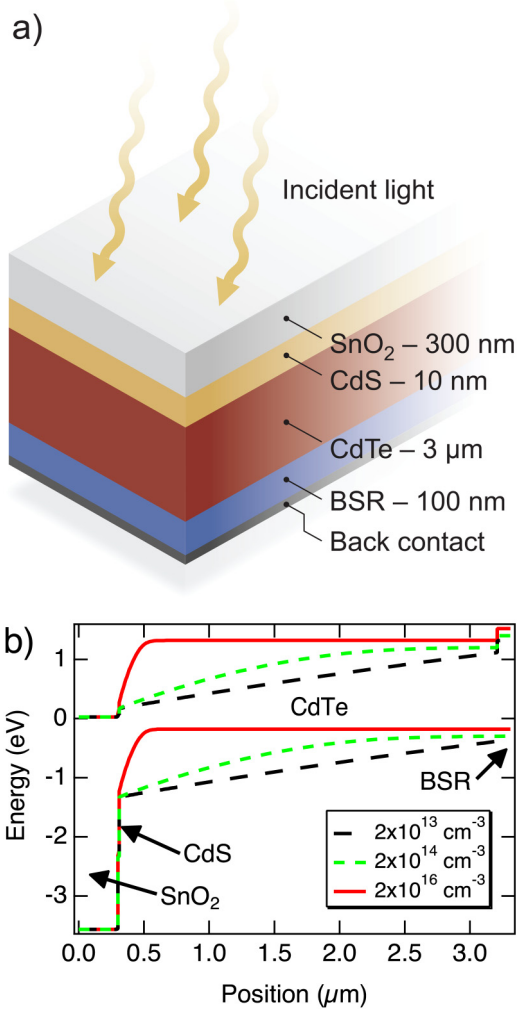

FIG. 1. (a) Device structure used for the simulations in this work. (b) Band diagram for the modeled structure with a 0.2-eV BSR at three levels of absorber hole density.

from valence band bending rather than conduction band shifts and therefore are similar to results without a BSR.[27]

For typical Si solar cells, the depletion width is small relative to the absorber thickness, and the number of excess carriers is relatively small compared to the equilibrium carrier concentration in the quasi-neutral region. Consequently, minority-carrier lifetime is both a key driver in Si performance and a key part of solar research lexicon and thinking. Analytical equations for this case are well known and provide a strong conceptual framework. In contrast, for typical thin-film CdTe solar cells, the depletion region often extends throughout a large portion of the absorber thickness [Fig. 1(b)]. Assumptions and analytical solutions that hold for Si technology fail; yet, the classic framework is pervasive in

the thin-film literature. It is very difficult to produce analytical equations for the current density-voltage (JV) characteristics of lightly doped thin-film heterojunction solar cells. Limited analytical work has invoked strict assumptions on simplified structures and often focused on narrow electrical-bias ranges where closed solutions may be approximated. For example, to address solar cells where recombination in the depletion region can no longer be ignored, Fahrenbruch and Bube[28] describe a homojunction approach where the device recombination current is approximated by the product of a characteristic length ($kT/q\mathbf{E}$) and the maximum Shockley-Read-Hall (SRH) recombination rate in the depletion region, which is approximated to be where excess electrons and holes are equal. Sah, Noyce, and Shockley[29] and Choo[30] assume that quasi-Fermi levels are nearly constant throughout a homojunction depletion region to approximate and integrate recombination current. The results are generally not in closed form except for certain bias ranges, and, importantly, current-voltage expressions include both the majority- and minority-carrier lifetimes. The analytical challenges highlight that for lightly doped thin-film solar cells, the depletion region can extend throughout large regions of the absorber, and photoinjected and excess carriers can exceed the depleted hole density over a spatial region that varies as a function of the electrical bias and absorber hole density. Consequently, simulations are the most effective method to estimate performance for the wide range of experimental carrier concentrations and lifetimes examined here. JV and time-resolved photoluminescence (TRPL) measurements are simulated by simultaneously solving the Poisson equation and electron and hole continuity equations:

$$\nabla \cdot \mathbf{E} = \frac{q}{\varepsilon}(p - n + N_d - N_a), \tag{1}$$

$$\nabla \cdot \mathbf{J}_p = \nabla \cdot (q\mu_p p\mathbf{E} - qD_p \nabla p) = q\left(G - R - \frac{\partial p}{\partial t}\right), \tag{2}$$

and

$$\nabla \cdot \mathbf{J}_n = \nabla \cdot (q\mu_n n\mathbf{E} + qD_n \nabla n) = -q\left(G - R - \frac{\partial n}{\partial t}\right). \tag{3}$$

Here, q is the elementary electronic charge, ε is the electrical permittivity, n and p are the total free electron and hole densities, N_d and N_a are the ionized donor and acceptor concentrations, $\mathbf{J}_p$ and $\mathbf{J}_n$ represent the hole and electron current densities due to drift and diffusion, $\mathbf{E}$ is the electric field, D_p and D_n are the hole and electron diffusion coefficients, and μ_p and μ_n are the hole and electron mobilities, respectively. G describes the generation rate due to the incoming light in solar operation or a laser pulse for time-resolved experiments and R describes the total recombination rate. Here, this is set equal to the sum of radiative recombination and bulk and interfacial SRH recombination. Simulation results are generated using Sentaurus Device;[31] the current-voltage trends can be reproduced using SCAPS,[32] albeit with different photocurrent due to differences in how the optics are calculated.

III. RESULTS AND DISCUSSION

A. Impact of majority-carrier lifetime

Contrary to the classic Si model, for lightly doped thin-film absorbers, *both* majority- and minority-carrier recombination can drive performance and the degree to which carriers are affected by the back surface. The physical underpinning can be understood by examining the expression for SRH recombination given by[33,34]

$$R_{SRH} = \frac{pn - p_o n_o}{\tau_p[n + n_i e^{(E_t - E_i)/kT}] + \tau_n[p + n_i e^{(E_i - E_t)/kT}]}, \tag{4}$$

where n_i represents the intrinsic carrier density, E_t represents the energy level of a single trap, E_i represents the intrinsic energy level, and τ_p and τ_n represent the hole and electron SRH lifetimes, respectively. The total hole and electron densities, p and n, are given by

$$p = p_o + \Delta p \quad \text{and} \quad n = n_o + \Delta n, \tag{5}$$

where p_o and n_o are the equilibrium hole and electron densities and Δp and Δn are the excess hole and electron densities, respectively. Here, we consider p-type material, $p_o \gg n_o$, and mid-gap centers such that the n_i terms are relatively small. Equation (4) can be rewritten as

$$R_{SRH} \approx \frac{p_o \Delta n + \Delta p \Delta n}{\tau_n[p_o + \Delta p] + \tau_p \Delta n}. \tag{6}$$

In low-injection conditions, $p_o \gg \Delta p$ or Δn and Eq. (6) reduces to

$$R_{SRH} \approx \Delta n/\tau_n. \tag{7}$$

Hence, the minority-carrier lifetime determines the SRH recombination rate. On the other hand, in high-injection conditions where Δn or $\Delta p \gg p_o$, Eq. (6) reduces to

$$R_{SRH} \approx \Delta n/(\tau_n + \tau_p), \tag{8}$$

and the effective lifetime is determined by the *sum* of the minority- and majority-carrier lifetimes. Conceptually, holes must also be captured to complete electron-hole recombination in high injection.

Consequently, for lightly doped material, majority-carrier lifetime becomes important. However, is there a path to estimate it? For thin-film materials, lifetime is typically measured by TRPL.[35] The minority-carrier lifetime can be measured in low-injection conditions by reducing the laser power so that the number of injected carriers is less than the equilibrium carrier concentration in a suitable test structure, such as a

CIGS absorber layer prior to device completion. By fitting TRPL decay curves in high-injection conditions on devices after initial laser, drift, and diffusion transients, for injection levels where radiative and Auger recombination are small compared to SRH recombination, the sum of the minority- and majority-carrier lifetime can be estimated.

Baseline CIGS and CdTe models often used by the thin-film community have held τ_p at values as high as 500 ns to 1 μs. These values, intended as a starting point but generally not changed in later work, can impact the projected effects and resulting efforts on back-surface passivation and reflectors.[11,32,36,37] In practice, it is possible to determine whether a device model reproduces observed experimental TRPL data by comparison to the above equations or to TRPL simulations. If a material has a minority-carrier lifetime of 1 ns and a majority-carrier lifetime of 500 ns, then the measured high-injection TRPL lifetime after initial laser and diffusion transients should equal nearly 500 ns. To illustrate this behavior, we simulate TRPL curves by solving the time-resolved form of Eqs. (1)–(3).[10,18,25] Similar to experimental measurements, a modeled laser pulse with a 500-fs half-width and a wavelength of 650 nm injects electron-hole pairs after passing through the front contact and buffer layers onto a CdTe absorber with a hole density of 2×10^{14} cm^{-3}. Simulated TRPL decay curves are compared for τ_p values of 1 ns and 500 ns with τ_n fixed at 1 ns. Figure 2 illustrates that the resulting TRPL decay curve for $\tau_p = 500$ ns is about two orders of magnitude greater than experimental TRPL decay curves measured on typical devices.[25] The condition with $\tau_n = \tau_p = 1$ ns, however, demonstrates a faster decay more consistent with early TRPL experiments on CdTe PV,[38] and generally, a more accurate representation of experimental recombination kinetics. Earlier models setting minority- and majority-carrier lifetimes equal have reproduced curves between fitted TRPL lifetimes and solar cell open-circuit voltage.[39]

To examine how majority-carrier lifetime can influence the predicted role of back-contact recombination and a BSR, we compare JV simulation results for $\tau_p = \tau_n$ and $\tau_p \gg \tau_n$. In Fig. 3(a), the CdTe and BSR hole-density values are 2×10^{13} cm^{-3}, $\tau_n = 1$ ns, and τ_p is compared at 1 ns and 500 ns. JV curves are shown for φ_e from 0 to 0.2 eV. For $\tau_p = 500$ ns, the BSR has a pronounced effect, increasing V_{oc} from 816 mV to a surprising 956 mV with a corresponding efficiency of 23.2%, despite low hole density and short minority-carrier lifetime. However, the strong performance boost is predicted only for a τ_p value significantly greater than is commonly measured by TRPL in typical PX CdTe solar cells. When $\tau_p = 1$ ns, the efficiency is just 9.2% with a modest V_{oc} of 736 mV, and the JV curves demonstrate no significant advantage in using a BSR. Clearly, majority-carrier lifetime is important.

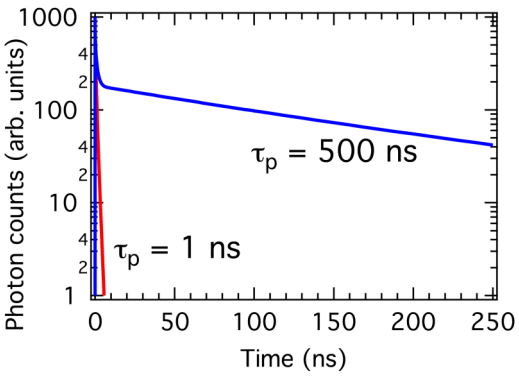

FIG. 2. TRPL simulation with 1-ns and 500-ns hole lifetimes.

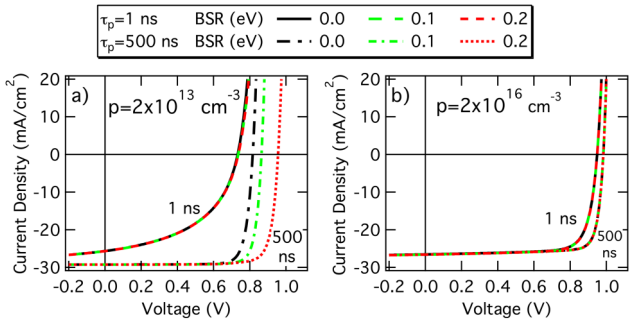

FIG. 3. Modeled JV curves with $S_b = 1\times10^7$ cm/s, $\tau_n = 1$ ns, and φ_e from 0 to 0.2 eV. (a) CdTe and BSR with $p = 2\times10^{13}$ cm^{-3} and τ_p of 1 and 500 ns. The 1-ns curves for the three φ_e values overlap one another. (b) Results for $p = 2\times10^{16}$ cm^{-3}. The 1-ns curves and the 500-ns curves for the three BSR levels overlap one another, respectively.

Figure 3(b) illustrates the results for a BSR when the CdTe hole density is 2×10^{16} cm^{-3}, typical for effective GrV doping. In agreement with earlier results,[24] neither the $\tau_p = \tau_n$ model nor the $\tau_p \gg \tau_n$ model indicates any significant BSR advantage in this case.

B. Back-surface passivation

Back-surface passivation and reflectors may be important due to the significant hole density and lifetime improvements emerging in CdTe and present in other thin-film technologies. Figures 4 and 5 illustrate how power conversion efficiency varies as electron and hole lifetime increase together ($\tau_n = \tau_p$) from 1 to 500 ns in conjunction with different front- and back-interface recombination velocities. Figure 4 examines passivating the back contact without a BSR. The surface recombination velocity at the absorber interface with the window layer, S_{front}, is considered for both an ideal interface ($S_{front} = 0$ cm/s) and a typical value of $S_{front} = 10^5$ cm/s.[10,40,41] S_b is varied from 10^3 to 10^7 cm/s to illustrate the role of passivation at the back absorber interface. If the lifetime is less than about 10 ns, which is common for PX CdTe devices, there is no significant advantage to passivating the back surface regardless of the front-interface recombination velocity.

For the $p = 2\times10^{14}$ cm^{-3} case [Fig. 4(a)] with an ideal front interface and lifetimes ranging from 50 ns to 500 ns,

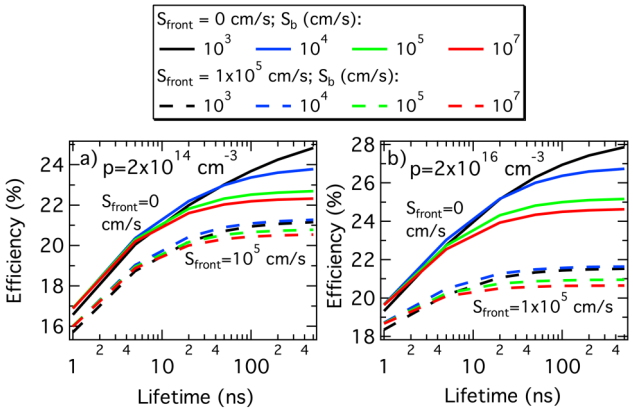

FIG. 4. Efficiency vs. bulk lifetime calculated for S_{front} values of 0 and 10^5 cm/s and S_b ranging from 10^3 to 10^7 cm/s without a BSR. (a) $p = 2 \times 10^{14}$ cm^{-3} case. (b) $p = 2 \times 10^{16}$ cm^{-3} case.

back-surface passivation can increase absolute efficiency by 3% to values as high as 25%. Interestingly, the benefits are much smaller for $S_{front} = 10^5$ cm/s, where maximum efficiency is 21% and back-surface passivation provides at most a 1% improvement.

For $p = 2 \times 10^{16}$ cm^{-3} [Fig. 4(b)] and $S_{front} = 10^5$ cm/s, the efficiency is limited to 22%, demonstrating that the front-interface recombination can prevent efficiency gains despite a two-order increase in the hole density. For $S_{front} = 10^5$ cm/s, back-surface passivation provides at most a 1.5% improvement. Adjusting S_{front} from 10^5 to 0 cm/s increases potential efficiency from about 21%–22% to 24%–28%. Back-surface passivation may increase absolute efficiency by

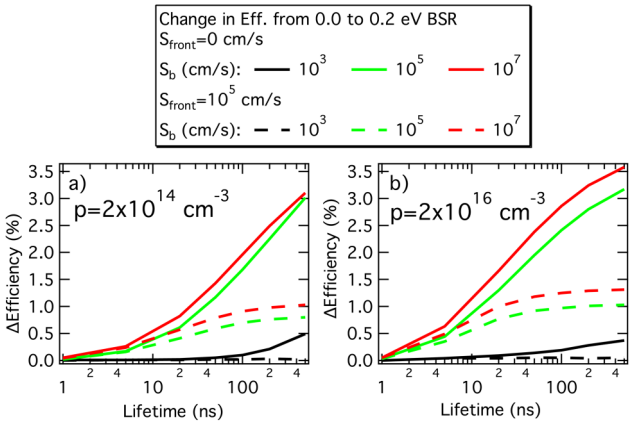

FIG. 5. Change in absolute cell efficiency between a 0.2-eV BSR and no BSR as a function of electron and hole lifetime for CdTe with (a) $p = 2 \times 10^{14}$ cm^{-3} and (b) 2×10^{16} cm^{-3}, $S_{front} = 0$ cm/s or 10^5 cm/s, and S_b ranging from 10^3 to 10^7 cm/s.

1% to 4% as lifetime increases from 10 to 500 ns. Thus, efforts to improve front-interface passivation and absorber hole density and lifetime should precede back-contact improvements. Efficiencies of 28% are calculated for an ideal front interface, bulk lifetimes approaching several hundred ns, and $S_b \leq 10^3$ cm/s. Although difficult in practice, the latter two values have recently been reported in PX $CdSe_xTe_{1-x}$ double heterostructures.[42]

C. Back-surface reflector

To examine the benefits of a BSR, Fig. 5 illustrates the change in absolute efficiency as a function of lifetime for low and high hole-density values and a range of S_b values. The BSR height is 0.2 eV. If the back surface is well passivated, a BSR is not significantly advantageous. For example, for $S_{front} = 0$ cm/s (solid lines) and $S_b = 10^3$ cm/s, the maximum BSR absolute efficiency gains for both $p = 2 \times 10^{14}$ cm^{-3} [Fig. 5(a)] and $p = 2 \times 10^{16}$ cm^{-3} [Fig. 5(b)] are minimal below 100 ns and limited to 0.5% at 500 ns. For $S_{front} = 10^5$ cm/s (dashed lines), no efficiency gain is observed for either hole-density value when $S_b = 10^3$ cm/s.

The BSR produces measurable absolute efficiency gains if there is substantive back-surface recombination. The degree is again regulated by front-interface recombination that can inhibit minority carriers from reaching the back surface. For $S_b \geq 10^5$ cm/s, $S_{front} = 10^5$ cm/s, and $p = 2 \times 10^{14}$ cm^{-3} or 2×10^{16} cm^{-3}, absolute efficiency gains are limited to <1.5% even for very long 500-ns bulk lifetimes. Without front-interface recombination, as lifetime increases from 1 to 500 ns, a BSR can provide absolute efficiency gains ranging from 0% to 3.5% and another route to 28% efficiency.

IV. CONCLUSIONS

The results demonstrate the degree to which back-surface passivation and reflectors can improve performance as a function of emerging absorber and interface properties, as well as how the physics of lightly doped thin-film solar cells requires careful consideration of majority-carrier lifetime and lifetime values that are consistent with experiment. In the case of CdTe, the data indicate that for ordinary PX lifetimes up to 10 ns and/or front-interface recombination velocities of 10^5 cm/s, back-surface passivation and reflectors will yield small changes that can be difficult to detect. A practical approach is to focus on improving the front-interface recombination velocity and the absorber first, then implementing the back-surface passivation or reflector that will ultimately be critical to improving efficiency beyond 25%. The simulations and recent measurements for hole density, lifetime, and interface recombination indicate that thin-film technologies such as CdTe have plausible paths to ultimately achieve 28% cell efficiency.

SUPPLEMENTARY MATERIAL

See supplementary material for a table of parameter values used in the CdTe device model.

ACKNOWLEDGMENTS

This work was authored by the National Renewable Energy Laboratory, operated by Alliance for Sustainable Energy, LLC, for the U.S. Department of Energy (DOE) under Contract No. DE-AC36-08GO28308, funded by the U.S. DOE Office of Energy Efficiency and Renewable Energy Solar Energy Technologies Office. The views expressed in the article do not necessarily represent the views of the DOE or the U.S. Government. The U.S. Government retains and the publisher, by accepting the article for publication, acknowledges that the U.S. Government retains a nonexclusive, paid-up, irrevocable, worldwide license to publish or reproduce the published form of this work, or allow others to do so, for U.S. Government purposes.

REFERENCES

[1]National Renewable Energy Laboratory, *Research Cell Record Efficiency Chart*, see https://www.nrel.gov/pv/assets/pdfs/pv-efficiency-chart.20181221.pdf
[2]K. L. Schulte, A. Braun, J. Simon, and A. J. Ptak, Appl. Phys. Lett. **112**, 042101 (2018).
[3]C. Yan, J. Huang, K. Sun, S. Johnston, Y. Znang, H. Sun, A. Pu, M. He, F. Liu, K. Eder, L. Yang, J. M. Cairney, N. J. Ekins-Daukes, Z. Hameiri, J. A. Stride, S. Chen, M. A. Green, and X. Hao, Nat. Energy **3**, 764 (2018).
[4]D. Feldman, J. Hoskins, and R. Margolis, Q4 2017/Q1 2018 *Solar Industry Update*, see https://www.nrel.gov/docs/fy18osti/71493.pdf (last accessed August 9, 2018).
[5]*Lazard's Levelized Cost of Energy Analysis—Version 11.0*, 2017, see https://www.lazard.com/media/450337/lazard-levelized-cost-of-energy-version-110.pdf (last accessed August 9, 2018).
[6]A. H. Munshi, J. Kephart, A. Abbas, J. Raguse, J.-N. Beaudry, K. Barth, J. Sites, J. Walls, and W. Sampath, IEEE J. Photovolt. **8**(1), 310 (2018).
[7]D. E. Swanson, J. R. Sites, and W. S. Sampath, Sol. Energy Mater. Sol. Cells **159**, 389 (2017).
[8]N. R. Paudel and Y. Yan, Appl. Phys. Lett. **105**, 183510 (2014).
[9]M. A. Green, Y. Hishikawa, E. D. Dunlop, D. H. Levi, J. Hohl-Ebinger, and A. W. Y. Ho-Baillie, Prog. Photovolt. Res. Appl. **26**, 427 (2018).
[10]A. Kanevce, M. O. Reese, T. M. Barnes, S. A. Jensen, and W. K. Metzger, J. Appl. Phys. **121**, 214506 (2017).
[11]J. R. Sites and J. Pan, Thin Solid Films **515**, 6099 (2007).
[12]J. N. Duenow, J. M. Burst, D. S. Albin, D. Kuciauskas, S. W. Johnston, R. Reedy, and W. K. Metzger, Appl. Phys. Lett. **105**(5), 053903 (2014).
[13]J. M. Burst, J. N. Duenow, D. S. Albin, E. Colegrove, M. O. Reese, J. A. Aguiar, C.-S. Jiang, M. K. Patel, M. M. Al-Jassim, D. Kuciauskas, S. Swain, T. Ablekim, K. G. Lynn, and W. K. Metzger, Nat. Energy **1**, 16015 (2016).
[14]Y. Zhao, M. Boccard, S. Liu, J. Becker, X.-H. Zhao, C. M. Campbell, E. Suarez, M. B. Lassise, Z. Holman, and Y.-H. Zhang, Nat. Energy **1**, 16067 (2016).
[15]J. M. Burst, S. B. Farrell, D. S. Albin, E. Colegrove, M. O. Reese, J. N. Duenow, D. Kuciauskas, and W. K. Metzger, APL Mater. **4**, 116102 (2016).
[16]E. Colegrove, J.-H. Yang, S. P. Harvey, M. R. Young, J. M. Burst, J. N. Duenow, D. S. Albin, S.-H. Wei, and W. K. Metzger, J. Phys. D Appl. Phys. **51**, 075102 (2018).
[17]B. E. McCandless, W. A. Buchanan, C. P. Thompson, G. Sriramagiri, R. Lovelet, J. Duenow, D. Albin, E. Colegrove, J. Moseley, H. Moutinho, S. Harvey, M. Al-Jassim, and W. K. Metzger, Sci. Rep. **8**, 14519 (2018).
[18]M. Amarasinghe, E. Colegrove, J. Moseley, H. Moutinho, D. Albin, J. Duenow, S. Jensen, J. Kephart, W. Sampath, S. Sivananthan, M. Al-Jassim, and W. Metzger, Adv. Energy Mat. **2018**, 1702666 (2018).
[19]M. Amarasinghe, E. Colegrove, H. Moutinho, D. Albin, J. Duenow, S. Johnston, J. Kephart, W. Sampath, M. Al-Jassim, S. Sivananthan, and W. K. Metzger, IEEE J. Photovolt. **8**(2), 600 (2018).
[20]M. Gloeckler, I. Sankin, and Z. Zhao, IEEE J. Photovolt. **3**(4), 1389 (2013).
[21]J. M. Kephart, A. Kindvall, D. Williams, D. Kuciauskas, P. Dippo, A. Munshi, and W. S. Sampath, IEEE J. Photovolt. **8**(2), 587 (2018).
[22]W. K. Metzger, I. L. Repins, and M. A. Contreras, Appl. Phys. Lett. **93**(2), 022110 (2008).
[23]S. D. Stranks, G. E. Eperon, G. Grancini, C. Menelaou, M. J. Alcocer, T. Teijtens, L. M. Herz, A. Petrozza, and H. J. Snaith, Science **342**, 341 (2013).
[24]K.-J. Hsiao, Sol. Energy Mater. Sol. Cells **120B**, 647 (2014).
[25]W. K. Metzger, R. K. Ahrenkiel, J. Dashdorj, and D. J. Friedman, Phys. Rev. B **71**, 035301 (2005).
[26]J. N. Duenow, J. M. Burst, D. S. Albin, M. O. Reese, S. A. Jensen, S. W. Johnston, D. Kuciauskas, S. K. Swain, T. Ablekim, K. G. Lynn, A. L. Fahrenbruch, and W. K. Metzger, IEEE J. Photovolt. **6**(6), 1641 (2016).
[27]J. Pan, M. Gloeckler, and J. R. Sites, J. Appl. Phys. **100**, 124505 (2006).
[28]A. L. Fahrenbruch and R. H. Bube, *Fundamentals of Solar Cells: Photovoltaic Solar Energy Conversion* (Academic Press, New York, 1983).
[29]C. T. Sah, R. N. Noyce, and W. Shockley, Proc. IRE **45**, 1228 (1957).
[30]S. C. Choo, Solid-State Electron. **11**(11), 1069 (1968).
[31]*Sentaurus Device Manual, Release I-2013.12* (Synopsys, Inc., 2013).
[32]M. Burgelman, P. Nollet, and S. Degrave, Thin Solid Films **361–362**, 527 (2000).
[33]W. Shockley and W. T. Read, Phys. Rev. **87**(5), 835 (1952).
[34]R. N. Hall, Phys. Rev. **87**(2), 387 (1952).
[35]R. K. Ahrenkiel and M. S. Lundstrom, *Minority Carriers in III-V Semiconductors: Physics and Applications* (Academic Press, San Diego, CA, 1993).
[36]N. Touafek and R. Mahamdi, Int. J. Renew. Energy Res. **4**(4), 958 (2014).
[37]M. Gloeckler, A. L. Fahrenbruch, and J. R. Sites, in *Proceedings of the 3rd World Conf. on Photovoltaic Energy Conversion* (IEEE, Osaka, 2003).
[38]W. K. Metzger, D. Albin, D. Levi, P. Sheldon, X. Li, B. M. Keyes, and R. K. Ahrenkiel, J. Appl. Phys. **94**(5), 3549 (2003).
[39]W. K. Metzger, M. J. Romero, P. Dippo, and M. Young, in *Proceedings of the 4th World Conference on Photovoltaic Energy Conversion* (IEEE, Waikoloa, HI, 2006).
[40]M. O. Reese, C. L. Perkins, J. M. Burst, S. Farrell, T. M. Barnes, S. W. Johnston, D. Kuciauskas, T. A. Gessert, and W. K. Metzger, J. Appl. Phys. **118**, 155305 (2015).
[41]M. O. Reese, J. M. Burst, C. L. Perkins, A. Kanevce, S. W. Johnston, D. Kuciauskas, T. M. Barnes, and W. K. Metzger, IEEE J. Photovolt. **5**(1), 382 (2015).
[42]D. Kuciauskas, J. M. Kephart, J. Moseley, W. K. Metzger, W. S. Sampath, and P. Dippo, Appl. Phys. Lett. **112**, 263901 (2018).